Inorg. Chem. **2003**, *42*, 8171–8180

A New Class of Oxo-Bridged High-Valent Hexamanganese Clusters Supported by Sterically Hindered Carboxylate Ligands

Sumitra Mukhopadhyay,[†] Bhavesh A. Gandhi,[†] Martin L. Kirk,*[,‡] and William H. Armstrong*[,†]

Departments of Chemistry, Eugene F. Merkert Chemistry Center, Boston College, 2609 Beacon Street, Chestnut Hill, Massachusetts 02467-3860, and The University of New Mexico, MSC03 2060, 1 University of New Mexico, Albuquerque, New Mexico 87131-0001

Received June 9, 2003

A new class of oxo-bridged high-valent hexamanganese (Mn_6) clusters containing a novel $\{Mn_6O_8\}^{6+}$ core, $[Mn^{IV}_4Mn^{III}_2(\mu\text{-}O)_4(\mu_3\text{-}O)_4(dmb)_6(O_2CR)_2]^{4+}$ (where dmb = 4,4′-dimethyl-2,2′-bipyridine, and RCO_2 = 2,6-di(*p*-tolyl)benzoate ($Ar^{Tol}CO_2^-$) (**3**) or 2,6-di(4-*tert*-butylphenyl)benzoate ($Ar^{4-tBuPh}CO_2^-$) (**4**)), was synthesized using sterically hindered *m*-terphenyl-derived carboxylate ligands. These complexes can be synthesized by oxidizing the Mn^{II} mononuclear complexes, $[Mn(dmb)_2(OH_2)(O_2CR)]^+$ (where $RCO_2 = Ar^{Tol}CO_2^-$ (**1**) or $Ar^{4-tBuPh}CO_2^-$ (**2**)) with (n-Bu_4N)MnO_4, by direct Mn(II) + Mn(VII) *in situ* comproportionation reactions, or by ligand substitution on the dinuclear manganese (III,IV) or (IV,IV) complexes, $[(Mn_2(\mu\text{-}O)_2(dmb)_4)]^{3+/4+}$. The compound $[Mn^{IV}_4Mn^{III}_2(\mu\text{-}O)_4(\mu_3\text{-}O)_4(dmb)_6(Ar^{Tol}CO_2)_2](OTf)_4$ [**3**$(OTf)_4$] crystallizes in the monoclinic space group $P2_1/n$, with the cell parameters a = 15.447(1) Å, b = 15.077(2) Å, c = 27.703(2) Å, β = 91.68(2)°, V = 6449.3(6) Å^3, and Z = 2. The X-ray structure reveals that there are three different bridging modes for the oxo groups: μ, "pyramidal" μ_3, and "T-shaped" μ_3. Solid-state variable temperature magnetic susceptibility studies suggest that the Mn centers are net antiferromagnetically coupled to yield a diamagnetic S_T = 0 ground spin state with a large number of low-lying, thermally accessible states with $S_T > 0$. ^{1}H NMR spectra were recorded for both Mn_6 clusters and selected resonances assigned. The electronic and redox properties of these complexes along with the effect of the presence of the bulky carboxylate ligands are also described here.

Introduction

Manganese is an essential redox-active element in biology, playing crucial roles in catalytic processes in many enzyme active sites including photosystem II (PSII) water oxidase (WO),[1,2] Mn-catalase,[3] Mn-superoxide dismutase (Mn-SOD),[4] and possibly Mn ribonucleotide reductase (Mn RRase).[5] The WO active site, in which resides an oxo-bridged tetranuclear manganese (Mn_4) complex, is responsible for the conversion of water to molecular oxygen. This process is the sole source of dioxygen on earth. Bacterial Mn-catalase has a binuclear manganese active site whereas manganese-dependent ribonucleotide reductase (*C. ammoniagenes* RRase)[6] and Mn-SOD were shown to contain a mononuclear Mn active site. In the field of bioinorganic chemistry, structural and functional modeling of these enzyme active sites involves synthesis of species containing up to four Mn ions. Nonetheless, modeling of the WO active site is most challenging, as the mechanism of oxygen evolution as well as the detailed structural properties of the manganese cluster are still poorly understood. This is due to the lack of high-resolution crystallographic data[7] and the inability to detect key reaction intermediates.[1]

* To whom correspondence should be addressed. E-mail: armstrow@bc.edu (W.H.A.); mkirk@unm.edu (M.L.K.).
† Boston College.
‡ University of New Mexico.

(1) Hoganson, C. W.; Babcock, G. T. *Met. Ions Biol. Syst.* **2000**, *37*, 613−656.
(2) Special dedicated issue, "Photosynthetic Water Oxidation": Nugent, J., Ed. *Biochim. Biophys. Acta* **2001**, *1503* (1−2), 1−259.
(3) (a) Yoder, D. W.; Hwang, J.; Penner-Hahn, J. E. *Met. Ions Biol. Syst.* **2000**, *37*, 527−557. (b) Barynin, V. V.; Whittaker, M. M.; Antonyuk, S. V.; Lamzin, V. S.; Harrison, P. M.; Artymiuk, P. J.; Whittaker, J. W. *Structure* **2001**, *9*, 725−738.
(4) Whittaker, J. W. *Met. Ions Biol. Syst.* **2000**, *37*, 587−611.
(5) Auling, G.; Follmann, H. *Met. Ions Biol. Syst.* **1994**, *30*, 131−161.
(6) (a) Griepenburg, U.; Blasczyk, K.; Kappl, R.; Hüttermann, J.; Auling, G. *Biochemistry* **1998**, *37*, 7992−7996. (b) Högbom, M.; Andersson, M. E.; Nordlund, P. *J. Biol. Inorg. Chem.* **2001**, *6*, 315−323 and references therein.
(7) (a) Zouni, A.; Witt, H.-T.; Kern, J.; Fromme, P.; Krauss, N.; Saenger, W.; Orth, P. *Nature* **2001**, *409*, 739−743. (b) Kamiya, N.; Shen, J.-R. *Proc. Natl. Acad. Sci. U.S.A.* **2003**, *100*, 98−103.

10.1021/ic034641h CCC: $25.00
Published on Web 11/04/2003

Most of these aforementioned enzymes that are characterized structurally harbor carboxylate-bridged Mn centers along with N-donor histidine ligands. In the absence of a well-resolved X-ray structure for the PSII active site, a multitude of biophysical techniques has been utilized in an effort to investigate the structure and immediate coordination environment of the Mn_4 cluster. In the context of ligands supporting the high oxidation state manganese ions, redox-resistant ligands such as bridging oxides, hydroxides, and carboxylate side-chains of amino acid residues have long been recognized. Site-directed mutagenesis studies show that the Mn_4 complex is bound predominantly to carboxylate containing amino acid residues (aspartate and glutamate) of the D1 polypeptide in PSII.[8] Recent crystallographic analyses also support that fact.[7b] Therefore, it is important to synthesize high-valent manganese complexes in the presence of carboxylate ligands in order to mimic the actual ligand environment of the WO active site.

High-valent manganese is also quite significant in material science because of its presence in octahedral molecular sieve catalysts[9] and because of the recent discovery of colossal magnetoresistance (CMR) observed in rare-earth perovskite magnetite systems,[10] $Ln_{1-x}A_xMnO_3$ (Ln = La, Pr, Nd, etc. and A = Ca, Sr, etc.). In addition, the recent discovery of single molecule magnets (SMMs)[11] has led to the design, synthesis, and magnetic characterization of large carboxylato-manganese clusters in search for systems that possess high-spin ground states and negative magnetic anisotropies. Generally, smaller carboxylate ligands such as acetate and benzoate have received the most attention in synthesizing such high-nuclearity complexes both in the presence and absence of O- and N-donor chelating ligands. Noteworthy complexes revealing SMM properties at low temperature ($\sim$2 K) include Mn_{12}[12] aggregates along with a few other systems with the following nuclearity: Mn_4,[14a] Mn_8,[14b] Mn_9,[14b,c] Mn_{10},[13a] Mn_{16},[13b] Mn_{18},[14d] and Mn_{30}.[14e]

It is quite common that the small carboxylates often accommodate a large number of Mn atoms, forming clusters with high nuclearity that have little importance from the biological point of view.[13−15] In order to restrict higher aggregation, here we take an approach of employing much bulkier carboxylate ligands. Others have applied sterically hindered *m*-terphenyl-derived carboxylate ligands to model non-heme diiron enzyme active sites, including methane monooxygenase and ribonucleotide reductase.[16−21] Until now, the use of such bulky substituted benzoate ligands in Mn coordination chemistry has been unexplored.

Our initial attempts in synthesizing high-valent oxo-manganese complexes with the bulky benzoate ligands, 2,6-di(*p*-tolyl)benzoate ($Ar^{Tol}CO_2^-$),[16−19,23] and 2,6-di(4-*tert*-butylphenyl)benzoate ($Ar^{4-tBuPh}CO_2^-$),[22] afforded a new class of hexamanganese clusters containing an unprecedented $\{Mn^{IV}_4Mn^{III}_2(\mu\text{-}O)_4(\mu_3\text{-}O)_4\}^{6+}$ core. In this paper, we describe the synthesis and characterization of these new Mn_6 complexes, $[Mn_6O_8(dmb)_6(O_2CR)_2]^{4+}$ (where dmb = 4,4′-dimethyl-2,2′-bipyridine, and RCO_2 = 2,6-di(*p*-tolyl)benzoate ($Ar^{Tol}CO_2^-$) (**3**) or 2,6-di(4-*tert*-butylphenyl)benzoate ($Ar^{4-tBuPh}CO_2^-$) (**4**)). Several other Mn_6 compounds with carboxylate and pyridine-based ligands have been reported in the past,[24−27] but complexes **3** and **4** are the first to have the core structure revealed here with such a high average Mn-ion oxidation state. Different synthetic routes for these clusters and their distinctive physical properties are provided in the following sections.

(8) (a) Magnuson, A.; Andréasson, L.-E. *Biochemistry* **1997**, *36*, 3254−3261. (b) Diner, B. A. *Biochim. Biophys. Acta* **2001**, *1503*, 147−163. (c) Debus, R. J. *Biochim. Biophys. Acta* **2001**, *1503*, 164−186.

(9) (a) Chen, X.; Shen, Y.-F.; Suib, S. L.; O'Young, C. L. *Chem. Mater.* **2002**, *14*, 940−948. (b) Corà, F.; Sankar, G.; Catlow, C. R. A.; Thomas, J. M. *Chem. Commun*. **2002**, 734−735.

(10) (a) Ju, H. L.; Kown, C.; Li, Qi.; Greene, R. L.; Venkatesan, T. *Appl. Phys. Lett*. **1994**, *65*, 2108−2110. (b) Kucherenko, S. S.; Pashchenko, V. P.; Polyakov, P. I.; Shtaba, V. A.; Shemyakov, A. A. *Low Temp. Phys.* **2001**, *27*, 559−562.

(11) Aromi, G.; Aubin, S. M. J.; Bolcar, M. A.; Christou, G.; Eppley, H. J.; Folting, K.; Hendrickson, D. N.; Huffman, J. C.; Squire, R. C.; Tsai, H.-L.; Wang, S.; Wemple, M. W. *Polyhedron* **1998**, *17*, 3005−3020.

(12) Thomas, L.; Lionti, F.; Ballou, R.; Gatteschi, D.; Sessoli, R.; Barbara, B. *Nature* **1996**, *383*, 145−147.

(13) (a) Kortus, J.; Baruah, T.; Bernstein, T.; Pederson, M. R. *Phys. Rev. B* **2002**, *66*, 092403/092401−092403/092404. (b) Price, D. J.; Batten, S. R.; Moubaraki, B.; Murray, K. S. *Chem. Commun*. **2002**, 762−763.

(14) (a) Yoo, J.; Brechin, E. K.; Yamaguchi, A.; Nakano, M.; Huffman, J. C.; Maniero, A. L.; Brunel, L.-C.; Awaga, K.; Ishimoto, H.; Christou, G.; Hendrickson, D. N. *Inorg. Chem.* **2000**, *39*, 3615−3623. (b) Boskovic, C.; Wernsdorfer, W.; Folting, K.; Huffman, J. C.; Hendrickson, D. N.; Christou, G. *Inorg. Chem.* **2002**, *41*, 5107−5118. (c) Brechin, E. K.; Soler, M.; Davidson, J.; Hendrickson, D. N.; Parsons, S.; Christou, G. *Chem. Commun.* **2002**, 2252−2253. (d) Brechin, E. K.; Boskovic, C.; Wernsdorfer, W.; Yoo, J.; Yamaguchi, A.; Sañudo, E. C.; Concolino, T. R.; Rheingold, A. L.; Ishimoto, H.; Hendrickson, D. N.; Christou, G. *J. Am. Chem. Soc*. **2002**, *124*, 9710−9711. (e) Soler, M.; Rumberger, E.; Folting, K.; Hendrickson, D. N.; Christou, G. *Polyhedron* **2001**, *20*, 1365−1369.

(15) (a) Low, D. W.; Eichhorn, D. M.; Draganescu, A.; Armstrong, W. H. *Inorg. Chem*. **1991**, *30*, 877−878. (b) Grillo, V. A.; Knapp, M. J.; Bollinger, J. C.; Hendrickson, D. N.; Christou, G. *Angew. Chem., Int. Ed. Engl*. **1996**, *35*, 1818−1820. (c) Sun, Z.; Gantzel, P. K.; Hendrickson, D. N. *Inorg. Chem*. **1996**, *35*, 6640−6641. (d) Brechin, E. K.; Clegg, W.; Murrie, M.; Parsons, S.; Teat, S. J.; Winpenny, R. E. P. *J. Am. Chem. Soc*. **1998**, *120*, 7365−7366.

(16) Lee, D.; Lippard, S. J. *J. Am. Chem. Soc*. **1998**, *120*, 12153−12154.

(17) Lee, D.; Du Bois, J.; Petasis, D.; Hendrich, M. P.; Krebs, C.; Huynh, B. H.; Lippard, S. J. *J. Am. Chem. Soc*. **1999**, *121*, 9893−9894.

(18) Lee, D.; Krebs, C.; Huynh, B. H.; Hendrich, M. P.; Lippard, S. J. *J. Am. Chem. Soc*. **2000**, *122*, 5000−5001.

(19) Lee, D.; Lippard, S. J. *J. Am. Chem. Soc*. **2001**, *123*, 4611−4612.

(20) (a) Hagadorn, J. R.; Que, L., Jr.; Tolman, W. B. *J. Am. Chem. Soc*. **1998**, *120*, 13531−13532. (b) Hagadorn, J. R.; Que, L., Jr.; Tolman, W. B.; Prisecaru, I.; Münck, E. *J. Am. Chem. Soc*. **1999**, *121*, 9760−9761.

(21) Tolman, W. B.; Que, L., Jr. *J. Chem. Soc., Dalton Trans*. **2002**, 653−660.

(22) Lee, D.; Sorace, L.; Caneschi, A.; Lippard, S. J. *Inorg. Chem*. **2001**, *40*, 6774−6781.

(23) Lee, D.; Hung, P.-L.; Spingler, B.; Lippard, S. J. *Inorg. Chem*. **2002**, *41*, 521−531.

(24) (a) Baikie, A. R. E.; Howes, A. J.; Hursthouse, M. B.; Quick, A. B.; Thornton, P. *Chem. Commun*. **1986**, 1587. (b) Schake, A. R.; Vincent, J. B.; Li, Q.; Boyd, P. D. W.; Folting, K.; Huffman, J. C.; Hendrickson, D. N.; Christou, G. *Inorg. Chem*. **1989**, *28*, 1915−1923.

(25) (a) Bhula, R.; Collier, S.; Robinson, W. T.; Weatherburn, D. C. *Inorg. Chem*. **1990**, *29*, 4027−4032. (b) Koehler, K.; Roesky, H. W.; Noltemeyer, M.; Schmidt, H. G.; Freire-Erdbruegger, C.; Sheldrick, G. M. *Chem. Ber*. **1993**, *126*, 921−926.

(26) (a) Kessissoglou, D. P.; Kampf, J.; Pecoraro, V. L. *Polyhedron* **1994**, *13*, 1379−1391. (b) Xia, X.; Verelst, M.; Daran, J.-C.; Tuchagues, J.-P. *Chem. Commun*. **1995**, 2155−2157.

(27) (a) Karsten, P.; Strahle, J. *Acta Crystallogr., Sect. C: Cryst. Struct. Commun.* **1998**, *54*, 1403−1406. (b) Abbati, G. L.; Cornia, A.; Fabretti, A. C.; Caneschi, A.; Gatteschi, D. *Inorg. Chem*. **1998**, *37*, 1430−1431.

Experimental Section

Materials. All chemicals were reagent grade and were used as obtained from commercial sources unless otherwise noted. Solvents CH_2Cl_2, THF, and CH_3CN were purified by passing through the activated alumina columns under argon (Modified Advanced Chem. Tech. Purification System). $Mn(OTf)_2 \cdot 2CH_3CN$[28a] and $(n\text{-}Bu_4N)MnO_4$[28b] were prepared according to the literature procedures. $[Mn_2(\mu\text{-}O)_2(dmb)_4](X)_n$ (where $n = 3$ and 4 and $X = ClO_4^-$ and OTf^-) complexes were synthesized in our laboratory as described previously.[29]

Caution: Perchlorate salts of metal complexes with organic ligands are potentially explosive and should be handled with care.

Physical Measurements. ^1H NMR spectra were recorded with Varian Unity 300 and 400 MHz spectrometers. Values for chemical shifts (ppm) are referenced to the residual solvent proton resonances (CHD_2CN, 1.94 ppm). IR spectra were recorded in the range 400−3500 cm^{-1} using a Nicolet 5DX FT-IR spectrometer using KBr disks. UV−vis spectra were recorded on a Hewlett-Packard diode array spectrophotometer (model HP8453) in the range 190−1100 nm. Mass spectral data were obtained using a Micromass LCT ESI mass spectrometer.

2,6-Di(*p*-tolyl)benzoate, Sodium Salt ($Ar^{Tol}CO_2Na$), and 2,6-Di(4-*tert*-butylphenyl)benzoate, Sodium Salt ($Ar^{4-tBuPh}CO_2Na$). These bulky carboxylate ligands were synthesized as described in the literature.[22,23]

$[Mn(dmb)_2(Ar^{Tol}CO_2)(OH_2)](X)$ [(1)(X), X = ClO_4^-, and $CF_3SO_3^-$]. To a light yellow acetonitrile solution (20 mL) of $Mn(CF_3SO_3)_2 \cdot 2CH_3CN$ (0.181 g, 0.416 mmol) or $Mn(ClO_4)_2 \cdot 6H_2O$ (0.151 g, 0.416 mmol) and dmb (0.153 g, 0.834 mmol) was added a methanol solution (10 mL) of $Ar^{Tol}CO_2Na$ (0.140 g, 0.432 mmol) with stirring. The solution color changed to brighter yellow. The reaction mixture was then evaporated to dryness, and the glassy yellow solid was crystallized from CH_2Cl_2/hexane to afford yellow blocks in 78−84% yield suitable for X-ray analysis. FTIR (KBr, cm^{-1}) for **1**(OTf): 3060 (w), 2930 (w), 1620 (vs), 1560 (vs), 1520 (m), 1490 (m), 1460 (m), 1412 (m), 1382 (m), 1285 (vs), 1222 (m), 1163 (s), 1031 (vs), 1015 (m), 922 (m), 829 (s), 800 (m), 768 (w), 741 (w), 702 (w), 638 (vs), 586 (w), 546 (m), 519 (s), 478 (w), 447 (w), 422 (w). Anal. Calcd for **1**(OTf)$\cdot 2CH_2Cl_2$, $C_{48}H_{47}Cl_4F_3MnN_4O_6S$: C, 54.30; H, 4.46; N, 5.28. Found: C, 53.41; H, 4.14; N, 5.11.

$[Mn(dmb)_2(Ar^{4-tBuPh}CO_2)(OH_2)](X)$ [(2)(X), X = ClO_4^-, and $CF_3SO_3^-$]. This compound was synthesized using the same procedure as described above, except $Ar^{4-tBuPh}CO_2Na$ was used instead of $Ar^{Tol}CO_2Na$. The product was crystallized from CH_2Cl_2/hexane providing 70−78% yield. FTIR (KBr, cm^{-1}) for **2**(OTf): 3380 (b, m), 3070 (w), 2971 (s), 2902 (w), 1620 (vs), 1560 (vs), 1512 (w), 1490 (m), 1453 (m), 1412 (m), 1382 (m), 1290 (vs), 1252 (vs), 1222 (m), 1163 (s), 1031 (vs), 1015 (s), 918 (m), 835 (s), 806 (m), 764 (m), 735 (s), 702 (w), 687 (w), 638 (s), 573 (m), 546 (m), 519 (m), 482 (m), 460 (vw), 402 (m). Anal. Calcd for **2**(OTf)$\cdot CH_2Cl_2$, $C_{53}H_{57}Cl_2F_3MnN_4O_6S$: C, 60.00; H, 5.42; N, 5.28. Found: C, 60.00; H, 5.22; N, 5.19.

$[Mn_6(\mu\text{-}O)_4(\mu_3\text{-}O)_4(dmb)_6(Ar^{Tol}CO_2)_2](X)_4$ [(3)(X)$_4$, X = ClO_4^-, and $CF_3SO_3^-$]. These compounds were synthesized by using three different methods.

Method A. Complexes **3**$(X)_4$ were synthesized directly in high yield by employing a "one-pot" comproportionation reaction between Mn(II) and Mn(VII) starting materials in the presence of the dmb and $Ar^{Tol}CO_2^-$ ligands. To a light yellow acetonitrile solution (30 mL) of $Mn(CF_3SO_3)_2 \cdot 2CH_3CN$ (0.270 g, 0.620 mmol) or $Mn(ClO_4)_2 \cdot 6H_2O$ (0.224 g, 0.620 mmol) and dmb (0.171 g, 0.930 mmol) was added a methanol solution (10 mL) of $Ar^{Tol}CO_2Na$ (0.101 g, 0.311 mmol) with stirring. The color of the solution changed to brighter yellow. To this solution was added an acetonitrile solution (~7 mL) of $(n\text{-}Bu_4N)MnO_4$ (0.113 g, 0.312 mmol) over a period of 10 min to provide a dark brown solution. It was stirred for another 30 min before the solvent was removed under reduced pressure. The resulting brown solid was extracted with ~30 mL of CH_2Cl_2. An insoluble white fraction was filtered off, and hexane was layered on top of the filtrate to afford dark brown crystals in 64−72% yield within a week. The dark crystalline product was collected by filtration. Brown hexagonal crystals of **3**$(OTf)_4$ suitable for X-ray crystallography were obtained by layering pentane carefully on top of a CH_2Cl_2 solution at room temperature. The purity of these complexes was confirmed by their ^1H NMR spectra, elemental analysis, and mass spectra (vide infra).

Method B. To an acetonitrile solution (20 mL) of **1** (0.336 mmol) was added slowly an acetonitrile solution (10 mL) of $(n\text{-}Bu_4N)MnO_4$ (0.062 g, 0.171 mmol) with stirring at room temperature. The color of the solution immediately changed to dark brown. Solvent was evaporated to dryness, and the compound was purified by following the same procedure already described. The yield was 62−68%. The purity of the complex was verified by ^1H NMR spectroscopy.

Method C. To an acetonitrile solution (10 mL) of $[Mn_2(\mu\text{-}O)_2(dmb)_4](X)_3$ (**5**) (0.075 mmol) was added a MeOH solution (5 mL) of $Ar^{Tol}CO_2Na$ (0.018 g, 0.055 mmol) dropwise, and the reaction mixture was stirred for 1 h under ambient conditions. The color changed from green to dark brown upon stirring. Solvent was evaporated to dryness, and the resulting brown solid was recrystallized from CH_2Cl_2/hexane to afford **3** in ~33−45% yield.

These complexes could also be synthesized by ligand substitution reactions on $[Mn_2(\mu\text{-}O)_2(dmb)_4](X)_4$ followed by aggregation using the similar procedure described above, only in these cases the reaction mixtures were stirred overnight as Mn(IV) is relatively inert toward ligand substitution reactions compared to Mn(III). The compounds were crystallized from CH_2Cl_2/hexane in 45−52% yield.

FTIR **3**$(OTf)_4$ (KBr, cm^{-1}): 1620 (vs), 1543 (s), 1491 (m), 1450 (s), 1413 (m), 1380 (s), 1273 (vs), 1222 (s), 1160 (s), 1036 (vs), 924 (m), 833 (s), 802 (m), 787 (w), 708 (w), 638 (vs), 604 (s), 586 (m), 544 (w), 519 (s), 461 (m), 428 (w). UV−vis **3**$(OTf)_4$ in CH_3CN, λ_{max}, nm (ϵ, M^{-1} cm^{-1}): 205 (2.90×10^5), 240 (1.79×10^5), and 301 (7.76×10^4). Anal. Calcd for **3**$(OTf)_4$, $C_{118}H_{106}F_{12}Mn_6N_{12}O_{24}S_4$: C, 51.31; H, 3.87; F, 8.25; Mn, 11.93; N, 6.09; S, 4.64. Found: C, 50.73; H, 3.82; F, 8.23; Mn, 11.92; N, 5.85; S, 4.55.

$[Mn_6(\mu\text{-}O)_4(\mu_3\text{-}O)_4(dmb)_6(Ar^{4-tBuPH}CO_2)_2](ClO_4)_4$ (4). This compound was synthesized in a manner similar to that described for **3** with methods A and B above, by in situ comproportionation reaction or by oxidizing **2**(ClO_4) with $(n\text{-}Bu_4N)MnO_4$. Slow evaporation of a CH_2Cl_2/toluene mixture afforded brown blocks of **4** in 50−55% yield.

FTIR **4** (KBr, cm^{-1}): 1617 (s), 1540 (m), 1491 (m), 1448 (m), 1410 (w), 1380 (s), 1304 (w), 1284 (w), 1247 (w), 1090 (vs), 1029 (s), 923 (m), 832 (s), 820 (w), 625 (s), 604 (s), 578 (m), 520 (m), 492 (w), 457 (w), and 430 (w). UV−vis (CH_3CN, λ_{max}, nm (ϵ, M^{-1} cm^{-1}): 205 (2.90×10^5), 240 (1.79×10^5), and 301 (7.76×10^4). Anal. Calcd for $C_{126}H_{130}N_{12}O_{28}Mn_6Cl_4$, $2CH_2Cl_2$: C, 52.98; H, 4.65; N, 5.79. Found: C, 52.93; H, 4.72; N, 5.77.

(28) (a) Bryan, P. S.; Dabrowiak, J. C. *Inorg. Chem.* **1975**, *14*, 296−299. (b) Sala, T.; Sargent, M. V. *Chem. Commun.* **1978**, 253−254.
(29) Mukhopadhyay, S.; Staples, R. J.; Armstrong, W. H. *Chem. Commun.* **2002**, 864−865.

X-ray Crystallographic Studies. Data were collected using a Bruker SMART-APEX CCD (charge coupled device) diffractometer equipped with an LT-3 low-temperature apparatus operating at 193 or 213 K. Suitable single crystals were chosen and mounted on a glass fiber using APIEZON-T grease. Data were measured using ω scans of 0.3° per frame for 30 s, such that a hemisphere was collected. A total of 1271 frames were collected with a maximum resolution of 0.75 Å. The first 50 frames were re-collected at the end of data collection to monitor for crystal decay. Crystals used for the diffraction studies showed no decomposition during data collection. Cell parameters were retrieved using SMART[30] software and refined using SAINT[31] on all observed reflections. Data reduction was performed using the SAINT software, which corrects for Lp and decay. Absorption corrections were done with the SADABS program,[35] supplied by George Sheldrick. The structures were solved by direct methods using the SHELXS-97[32] program and refined by least-squares methods on F^2 in SHELXL-97,[33] incorporated in SHELXTL-PC V 5.10.[34] All non-hydrogen atoms were refined with anisotropic thermal parameters. Hydrogen atom positions were calculated by geometrical methods and refined using a riding model. The structure of **1**(OTf) was solved in the orthorhombic space group *Pbca* after analysis of systematic absences. The current refinement gives two CH_2Cl_2 solvent molecules in the lattice, and on the basis of the Mn(1)−O(3) bond distance, we have modeled the Mn atom with a coordinated water molecule,[36−38] not a hydroxide anion. Compound **3**$(OTf)_4$ crystallizes in monoclinic space group $P2_1/n$. All drawings presented here are made using 30% probability thermal ellipsoids. Crystallographic information is provided in Tables 1 and 2.

Solid-State Magnetic Measurements. The isofield magnetic susceptibility of **3**$(OTf)_4$ was collected on a Quantum Design SQUID magnetometer between 2.0 and 300 K in an applied field of 0.5 T. The isothermal magnetization was also collected between 0 and 7 T at a temperature of 2 K. Molar paramagnetic susceptibilities were obtained by applying diamagnetic corrections calculated from Pascal's constants.[42,43]

Electrochemistry. A BAS-100B electrochemical analyzer was used for electrochemical measurements. A platinum disk working electrode and a platinum wire auxiliary electrode were used to collect cyclic voltammograms. A $Ag/AgClO_4$ electrode was used as reference electrode. Electrochemical measurements in acetonitrile were done in the presence of 0.1 M TBAP (tetrabutylammonium

Table 1. Summary of X-ray Crystallographic Data for Complexes **1** and **3**

	1(OTf)·$2CH_2Cl_2$	**3**$(OTf)_4$
empirical formula	$C_{48}H_{47}Cl_4F_3Mn$-N_4O_6S	$C_{118}H_{106}F_{12}Mn_6$-$N_{12}O_{24}S_4$
fw	1061.70	2762.03
T	193(2) K	213(2) K
wavelength	0.71073 Å	0.71073 Å
cryst syst	orthorhombic	monoclinic
space group	*Pbca*	$P2_1/n$
a, Å	18.000(3)	15.45(1)
b, Å	18.000	15.08(2)
c, Å	31.499 (5)	27.70(2)
β, deg	90	91.7(2)
V, Å^3	10205(2)	6449.3(6)
Z	8	2
D (calcd), Mg/m^3	1.382	1.422
abs coeff, mm^{-1}	0.570	0.723
cryst size, mm^3	0.08 × 0.06 × 0.05	0.15 × 0.10 × 0.08
θ limits, deg	1.72−28.39°	1.47−27.90
reflns collected	73498	40634
indep reflns	12708 [*R*(int) = 0.0494]	13555 [*R*(int) = 0.0945]
data/restraints/params	12708/0/604	13555/0/793
final *R* indices [$I > 2\sigma(I)$]	R1[a] = 0.0608, wR2[b] = 0.1715	R1[a] = 0.0770, wR2[b] = 0.2012
R indices (all data)	R1[a] = 0.0898, wR2[b] = 0.1876	R1[a] = 0.1599, wR2[b] = 0.2495
largest diff. peak and hole	1.245 and −0.945 e Å^{-3}	1.050 and −1.078 e Å^{-3}

[a] $R1 = \sum||2F_o| - |F_c||/\sum|F_o|$. [b] $wR2 = [\sum[w(|F_o|^2 - |F_c|^2)^2]/\sum[w(|F_o|^2)^2]]$.

Table 2. Selected Bond Lengths (Å) and Angles (deg) for **1** and **3**[a]

bond length		bond angle	
		1(OTf)·$2CH_2Cl_2$	
Mn(1)−O(2)	2.121(2)	O(1)−Mn(1)−N(3)	94.7(8)
Mn(1)−O(1)	2.174(2)	O(2)−Mn(1)−O(1)	88.11(7)
Mn(1)−N(4)	2.232(2)	O(1)−Mn(1)−N(4)	106.98(7)
Mn(1)−N(1)	2.246(2)	O(2)−Mn(1)−N(1)	106.76(7)
Mn(1)−N(3)	2.276(2)	O(1)−Mn(1)−N(1)	90.18(7)
Mn(1)−N(2)	2.272(2)	N(4)−Mn(1)−N(1)	156.74(8)
		O(1)−Mn(1)−N(2)	161.88(8)
		N(2)−Mn(1)−N(3)	89.05(8)
		3$(OTf)_4$	
Mn(1)−O(2)	1.817(4)	O(2)−Mn(1)−O(4)	102.6(2)
Mn(1)−O(4)	1.848(4)	O(2)−Mn(1)−O(4)A	95.1(2)
Mn(2)−O(1)	1.860(4)	O(4)−Mn(1)−O(4)A	82.9(2)
Mn(1)−O(1)	1.987(4)	O(2)−Mn(1)−O(1)	80.96(19)
Mn(1)−N(1)	2.065(5)	O(4)−Mn(1)−O(1)	84.07(19)
Mn(1)−N(2)	2.105(5)	O(4)A−Mn(1)−O(1)	165.2(2)
Mn(1)−Mn(1)A	2.765(2)	O(2)−Mn(1)−N(1)	88.4(2)
Mn(1)−Mn(2)	2.804(2)	O(1)−Mn(1)−N(1)	100.3(2)
Mn(1)−Mn(3)	3.033(1)	O(4)−Mn(1)−N(2)	92.6(2)
Mn(2)−O(3)	1.797(4)	O(1)−Mn(1)−N(2)	92.1(2)
Mn(2)−O(2)	1.826(3)	O(3)−Mn(3)−O(6)	89.7(2)
Mn(2)−O(1)	1.860(4)	O(1)−Mn(3)−O(6)	91.41(19)
Mn(2)−O(5)	1.954(3)	O(3)−Mn(3)−O(4)	91.01(19)
Mn(2)−N(3)	2.040(5)	O(1)−Mn(3)−O(4)	76.45(18)
Mn(2)−Mn(3)	2.634 (2)	N(6)−Mn(3)−O(4)	93.3(2)
Mn(3)−O(3)	1.812(4)	O(6)−Mn(3)−O(4)	167.8(2)
Mn(3)−O(1)	1.948(4)	Mn(1)−O(4)−Mn(3)	97.18(18)
Mn(3)−N(5)	2.041(5)	Mn(1)−O(4)−Mn(1)A	97.1 (2)
Mn(3)−N(6)	2.049(5)	Mn(1)−O(2)−Mn(2)	100.5 (2)
Mn(3)−O(6)	2.182(4)	Mn(2)−O(3)−Mn(3)	93.8 (2)
Mn(3)−O(4)	2.185(3)	Mn(2)−O(1)−Mn(3)	87.55 (19)

[a] Numbers in parentheses are estimated standard deviations of the last significant figure. Atoms are labeled as indicated in Figures 1 and 2.

(30) *SMART V 5.050 (NT) Software for the CCD Detector System*; Bruker Analytical X-ray Systems: Madison, WI, 1998.
(31) *SAINT V 5.01 (NT) Software for the CCD Detector System* Bruker Analytical X-ray Systems: Madison, WI, 1998.
(32) Sheldrick, G. M. *SHELXS-90, Program for the Solution of Crystal Structure*; University of Göttingen: Göttingen, Germany, 1990.
(33) Sheldrick, G. M. *SHELXL-97, Program for the Refinement of Crystal Structure*; University of Göttingen: Göttingen, Germany, 1997.
(34) *SHELXTL 5.10 (PC-Version), Program library for Structure Solution and Molecular Graphics*; Bruker Analytical X-ray Systems: Madison, WI, 1998.
(35) *SADABS*. Program for absorption corrections using Siemens CCD based on the method of Robert Blessing: Blessing, R. H. *Acta Crystallogr.* **1995**, *A51*, 33−38.
(36) Zhou, X.-H.; Yu, W.-T.; Wang, Z.-X.; Fu, Y.-J. *Z. Kristallogr.* **2000**, *215*, 496−498.
(37) McCann, M.; Casey, M. T.; Devereux, M.; Curran, M.; McKee, V. *Polyhedron* **1997**, *16*, 2741−2748.
(38) Cano, J.; Munno, G. D.; Sanz, J. L.; Ruiz, R.; Faus, J.; Lloret, F.; Julve, M.; Caneschi, A. *J. Chem. Soc., Dalton Trans.* **1997**, 1915−1923.
(39) Hagen, K. S.; Armstrong, W. H.; Olmstead, M. M. *J. Am. Chem. Soc.* **1989**, *111*, 774−775.
(40) Sañudo, E. C.; Grillo, V. A.; Knapp, M. J.; Bollinger, J. C.; Huffman, J. C.; Hendrickson, D. N.; Christou, G. *Inorg. Chem.* **2002**, *41*, 2441−2450.
(41) Sauer, K.; Yachandra, V. K. *Proc. Natl. Acad. Sci. U.S.A.* **2002**, *99*, 8631−8636.
(42) Mulay, L. N. In *Theory and Applications of Molecular Paramagnetism*; Boudreaux, E. A., Mulay, L. N., Eds.; Wiley: New York, 1976.
(43) Carlin, R. L. In *Magnetochemistry*; Springer-Verlag: Berlin, 1986.

Scheme 1. Synthesis of the Complexes

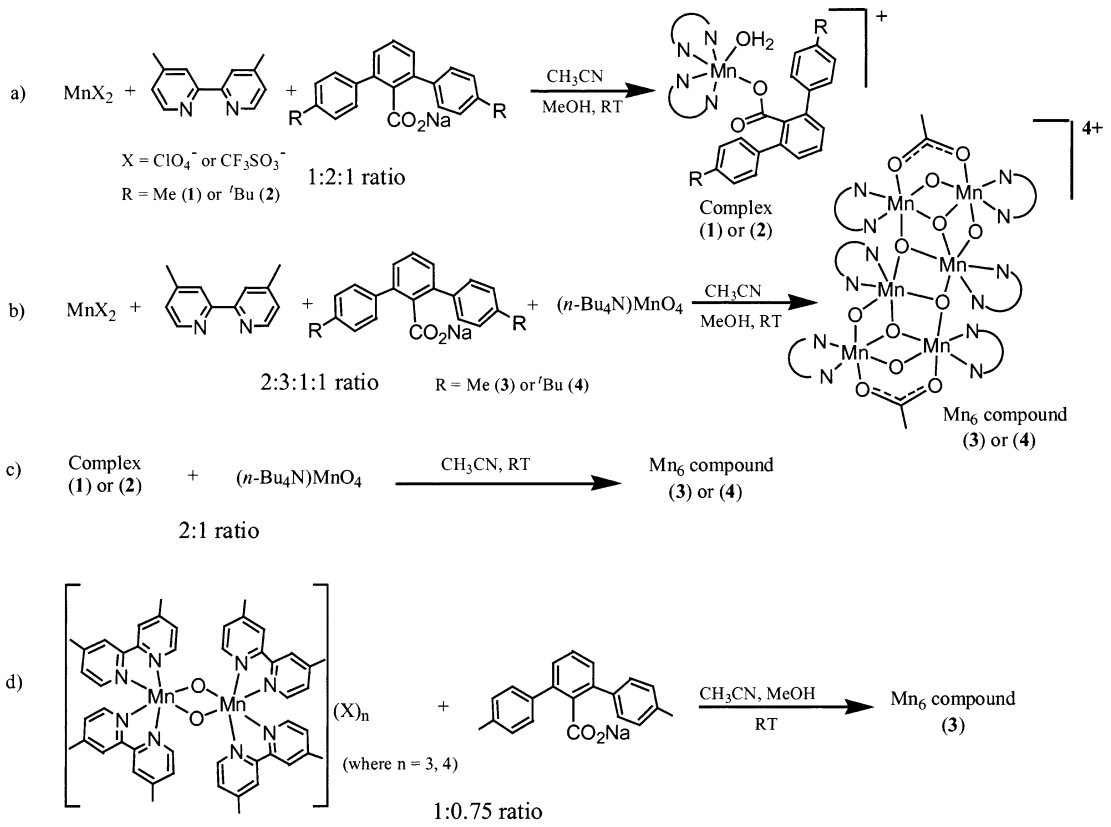

perchlorate) as supporting electrolyte. Under these conditions, the $E_{1/2}$ of the Fc/Fc^+ couple was 0.45 V (ΔE = ~70 mV). All electrochemical measurements were performed under a dry and purified dinitrogen atmosphere. The potentials reported in this work are uncorrected for junction contributions.

Results and Discussion

Synthesis and Structural Characterization of the Complexes. Reaction of MnX_2 (X = OTf and ClO_4), dmb (dmb = 4,4′-dimethyl-2,2′-bipyridyl), and $ArCO_2Na$ ($Ar^{Tol}CO_2^-$ = 2,6-di(*p*-tolyl)benzoate and $Ar^{4-tBuPh}CO_2^-$ = 2,6-di(4-*tert*-butylphenyl)benzoate) in acetonitrile in a 1:2:1 stoichiometric ratio gave the monomeric Mn(II) complexes **1** and **2** (Scheme 1a). Recrystallization from CH_2Cl_2/hexane afforded yellow crystals in good yield (75−85%). Complexes **3** and **4** were synthesized in acetonitrile by a comproportionation reaction between $Mn(X)_2$ and $(n\text{-}Bu_4N)MnO_4$ in the presence of dmb and $ArCO_2Na$ in a 2:1:3:1 ratio, respectively (Scheme 1b). Complexes **3** and **4** were also synthesized by oxidizing complexes **1** and **2**, with $(n\text{-}Bu_4N)MnO_4$ (2:1 ratio) in acetonitrile (Scheme 1c). Typically, **3** and **4** were obtained in modest to good yield (55−72%, based on Mn) following recrystallization from CH_2Cl_2/hexane and CH_2Cl_2/toluene, respectively.

Complex **3** was also prepared by ligand substitution on $[Mn_2(\mu\text{-}O)_2(dmb)_4](X)_n$ (where n = 3 or 4) with $Ar^{Tol}CO_2$-Na (~1:0.75 ratio) followed by aggregation to give the hexanuclear complex (Scheme 1d). However, this method provides much lower yields (~40−50%, based on Mn) with a yellow Mn(II) byproduct presumably as the result of a disproportionation reaction.

The crystal structure of **1**(OTf)·$2CH_2Cl_2$ is shown in Figure 1. Selected bond lengths and angles are listed in Table 2. Complex **1** has two dmb ligands coordinated to the Mn(II) center while the bulky carboxylate ($Ar^{Tol}CO_2$) is bound in a monodentate fashion. A water molecule occupies the sixth coordination site. The $Mn-O_{carboxylate}$ and $Mn-O_{water}$ distances are 2.121(2) and 2.174(2) Å, respectively, and are comparable to structurally analogous manganese complexes with aromatic carboxylate ligands reported previously.[36−38] The Mn−N bonds trans to the $Mn-O_{carboxylate}$ and $Mn-O_{water}$ bonds are slightly longer than the other two Mn−N bonds (~2.27 vs 2.24 Å). Similar observations have been reported

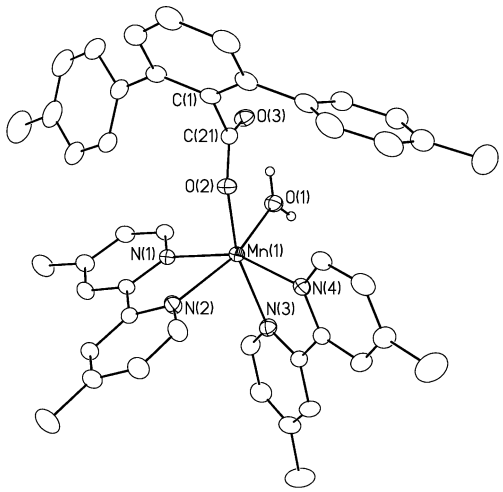

Figure 1. An ORTEP diagram of **1**(OTf)·$2CH_2Cl_2$ with thermal ellipsoids at 30% probability. (The H atoms, triflate counterion, and the solvent molecules are omitted for clarity.)

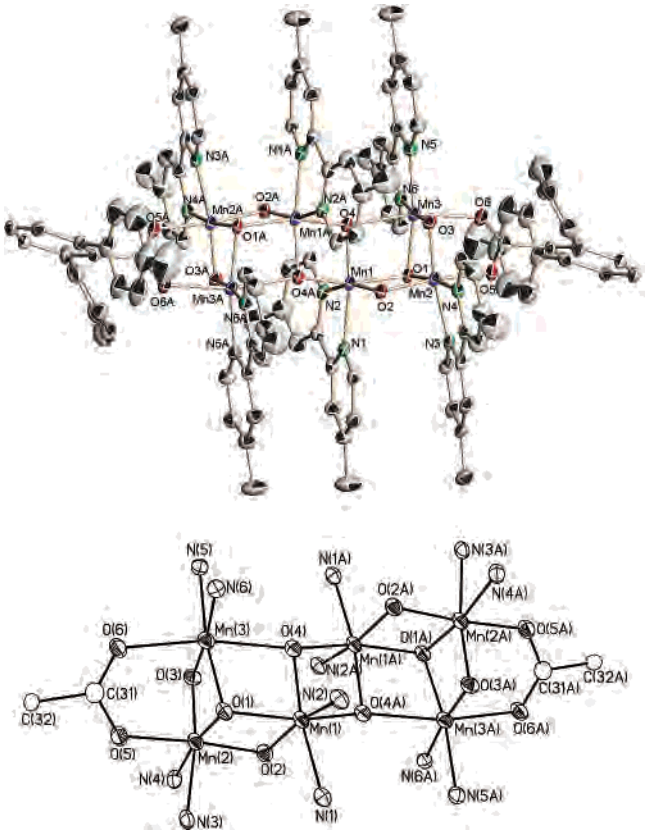

Figure 2. ORTEP diagrams of **3**$(OTf)_4$ with thermal ellipsoids at 30% probability: top, full cation; bottom, Mn_6 core. (The H atoms and the triflate counterions are omitted for clarity.)

in the literature.[36,37] Complex **2** was found to be isostructural to **1** (the crystallographic data are provided in the Supporting Information).

The X-ray crystal structure of **3** (Figure 2) demonstrates that the complex has a $\{Mn_6(\mu\text{-O})_4(\mu_3\text{-O})_4\}^{6+}$ core. Selected bond lengths and angles are listed in Table 2. Each Mn atom is connected to the other Mn atoms via two μ-oxo or μ_3-oxo groups, and the terminal two Mn centers on each end are also connected to each other by a bridging carboxylate ligand with a Mn···Mn separation of 2.634(2) Å. There are two different types of μ_3-O groups: two pyramidal ones with an av Mn−O−Mn angle of ∼95° and two rarely observed "T-shaped" μ_3-O groups with large Mn−O−Mn angle of ∼158°. The "T-shaped" μ_3-oxo groups are asymmetrical in terms of the Mn−O_{oxo} bond lengths (2.19 vs 1.84 Å) as they bind to both Mn(III) and Mn(IV) centers. Similar "T-shaped" triply bridging oxide ligands have been observed for a few other manganese clusters.[39,40]

Complex **3** has a crystallographic inversion center. Thus, the asymmetric unit contains only half of the molecule, a Mn_3O_4 moiety. The overall structure may be described as two cuboidal Mn_3 units connected by two "T-shaped" μ_3-oxo groups. There is a pyramidal μ_3-O atom {O(1) and O(1A)} in each half that connects all three Mn centers. Each of the four outermost Mn atoms {Mn(2), Mn(3), Mn(2A), and Mn(3A)} is bound to one dmb, and the inner two Mn atoms have two dmb ligands each (Scheme 2).

Assuming that all bridging O atoms are oxide groups (O^{2-}), that both the $Ar^{Tol}CO_2^-$ groups are deprotonated, and

Scheme 2. Schematic Diagram of the Mn_6 Core

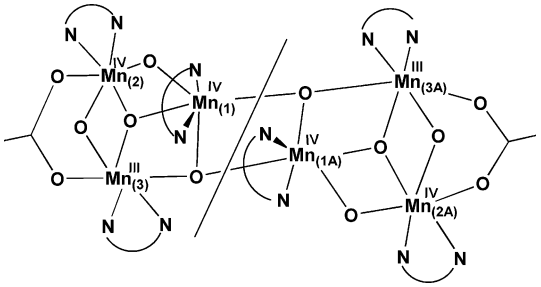

considering that the overall charge on the complex is 4+, four of the manganese atoms are deduced to be in the +4 oxidation state, and two of them in the +3 formal oxidation state. These Mn(IV) and Mn(III) centers can easily be distinguished by their Mn−O bond lengths on the basis of the fact that only the high-spin Mn(III) centers possess a Jahn−Teller (JT) distortion along their *z*-axes, resulting in elongated Mn−ligand bonds. Therefore, we assign Mn(1) and Mn(1A) (Scheme 2 and Figure 2) as +4 ions. This makes good chemical sense as they are bound to four oxo groups, which are harder donors compared to carboxylates and thus stabilize the higher oxidation state. On the basis of the ligand environments and metal−ligand bond distances, Mn(3) and Mn(3A) are assigned as +3 ions and Mn(2) and Mn(2A) as +4 ions. Mn(3) is bonded to two μ_3-oxo groups and has significantly longer Mn−O bonds than that of Mn(2), which is connected to only one μ_3-oxo group (Mn(3)−O(1) = 1.948(4) Å vs Mn(2)−O(1) = 1.860(4) Å, Mn(3)−O(4) = 2.185(3) Å vs Mn(2)−O(2) = 1.826(3) Å, and Mn(3)−O(6) = 2.182(4) Å vs Mn(2)−O(5) = 1.954(3) Å, the latter two Mn(3)−O bonds are considerably long because they are along the JT axis for Mn(3)). The distance between Mn(1) and Mn(2), (which are assigned as Mn(IV) centers) in one trinuclear unit is 2.804(2) Å, whereas the distance between $Mn(1)^{IV}$ and $Mn(3)^{III}$ is 3.033(1) Å. The distance between two Mn(IV) atoms (Mn(1) and Mn(1A)) from separate trinuclear units is 2.765(2) Å. The Mn(1)−O(2)−Mn(2) angle (between two Mn(IV) centers in a cuboidal unit) is ∼100°, whereas the Mn(2)−O(3)−Mn(3) angle (between the terminal Mn(IV) and Mn(III) center) is ∼93°. The crystal structure of **3** also reveals that the terminal bis-oxo-bridged Mn-dinuclear unit is in the same plane with the pyridine rings of the dmb ligands, which probably results from the steric constraint imposed by the bulky carboxylate ligands. The Mn_3O_4 cuboidal unit, as well as the tetranuclear moiety formed by Mn(1A), Mn(1), Mn(2), and Mn(3), are present in several proposed structures for the PSII active site (see in Figure 3).[41]

Though all our efforts to grow X-ray quality single crystals of **4** were unsuccessful, it was characterized by ^{1}H NMR, UV−vis, ESI-mass spectrometry and elemental analysis and deduced to have the same structure as **3**. The steric bulk on the carboxylate ligands apparently plays a critical role in assembling the $\{Mn_6(\mu\text{-O})_4(\mu_3\text{-O})_4\}^{6+}$ cores. To date, all of our attempts to synthesize such cores using acetate or unsubstituted benzoate ligands were unsuccessful. The encumbering bulk at the ortho positions of the benzoate ring

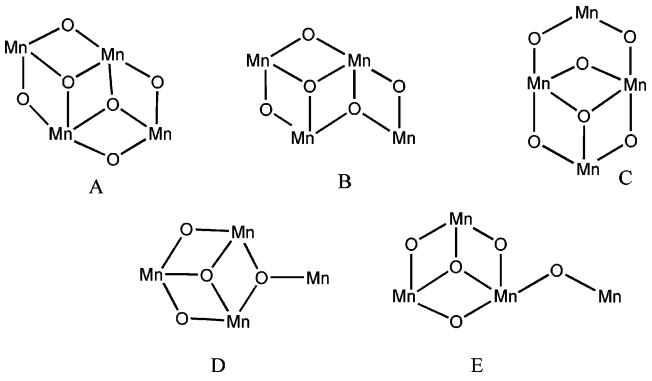

Figure 3. Proposed Mn_4 structures for PSII active site.

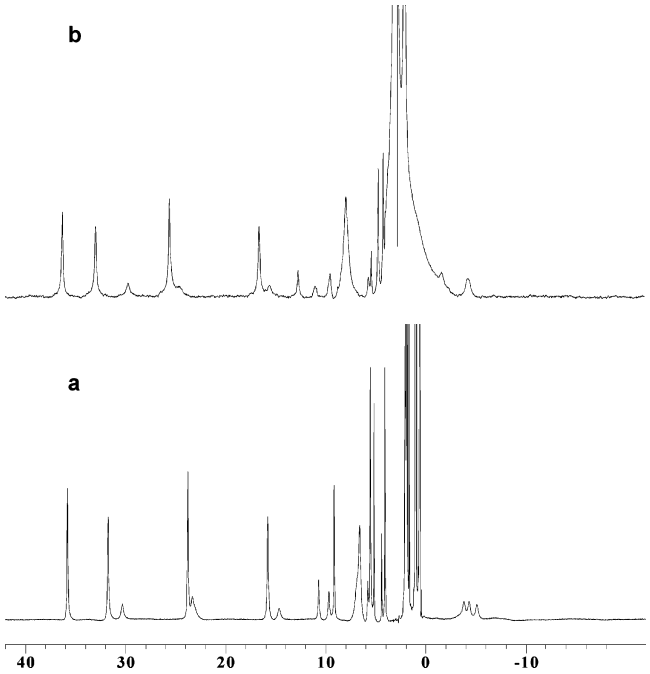

Figure 4. 300 MHz ^{1}H NMR spectra of complexes **3** (a) and **4** (b) in acetoniltile-d_3.

in the ligands used herein eliminates the possibility for the oxygen atoms of the carboxylates to bind to more than one Mn center simultaneously, thus preventing further branching through doubly or triply bridged $O_{carboxylate}$, which is the case for some polynuclear carboxylato-manganese clusters.[12−14] It is also a possibility, as apparent from the structure, that by capping the terminal Mn atoms these carboxylate ligands eliminate any further extension of the Mn_6 chain to result in higher aggregation or polymerization. Mass spectral data of the crude reaction mixture provide no evidence of the existence of any larger aggregates in solution other than the Mn_6 complex.

^{1}H NMR Spectroscopy. The ^{1}H NMR spectrum of **3** in CD_3CN suggests that it retains its solid-state structure in solution. Resonances are observed between −6 to +36 ppm, shown in Figure 4a. On the basis of the fact that the complex has an inversion center, one would expect six resonances for the methyl protons and 18 for aromatic ring protons of the dmb ligands. All six peaks assigned as methyl group protons (between 4 and 36 ppm) and at least 11 of 12 peaks consistent with the aromatic protons at dmb 3,3′ and 5,5′ pyridine ring positions are observed in the spectrum. The six 6,6′ protons are difficult to observe because of their close proximity to the paramagnetic centers. Also, the methyl groups and the aromatic protons of the carboxylate rings, which do not experience large shifts, as they are significantly distant from the Mn centers, are located between 1 and 7 ppm. The NMR spectrum of complex **4** shows features very similar to that of complex **3** (Figure 4b), confirming that it has the same core structure. The detailed assignments of the proton resonances for these Mn_6 complexes are provided in Table S1 in the Supporting Information.

Mass Spectrometry. The molecular ion (M^+) and the $M^{2+}/2$ ion peaks of **3**(ClO_4) are observed at 2463 and at 1182 amu, respectively, in the positive mode electrospray ionization mass spectrum. The distinctive isotope patterns of these two ion peaks, especially due to the presence of the perchlorate ion, match quite nicely with their simulated spectra, as depicted in Figure 5. The M^+ ion peak was not detected for **4** perhaps due to the fact that this is a somewhat larger cluster in terms of its external van der Waals boundary and, thus, anion dissociation occurs more readily under the same experimental conditions. The electrostatic attraction between cation and anion is expected to be less for **4** due to greater charge separation. However, the $M^{2+}/2$ ion peak with the proper isotope distribution was observed for **4**, and detailed analysis is provided in the Supporting Information (Figures S2 and S3).

IR Spectroscopy. IR spectra of **3** and **4** display strong absorptions at ∼1540 cm^{-1}, attributed to the O−C−O stretching vibrations of the bridging carboxylate ligands. The stretching vibrations for the N-donor ligands are also observed within the range 1600−1620 cm^{-1}. Intense bands for stretching vibrations of the $CF_3SO_3^-$ ions are observed at 1273 and 1036 cm^{-1}. The same is true for the ClO_4^- ions, for which vibrational bands are observed at ∼1090 and in the 615−635 cm^{-1} region.

Electronic Spectroscopy. Figure 6 displays the electronic spectrum of **3** in acetonitrile. Compounds **3** and **4** exhibit intense visible absorption bands at λ_{max} = 300−305 nm, which are tentatively assigned as LMCT transitions for the Mn^{IV}−oxo units. Two other intense bands appear at λ_{max} = 240−245 nm and λ_{max} = 202−205 nm, which are reasonably assigned as intraligand charge-transfer excitations. Although the complexes are dark brown in color, no discernable bands corresponding to d−d transitions have been resolved in the lower energy visible region.

Magnetism. The isofield dc magnetic data for **3**($OTf)_4$ were collected between 2 and 300 K in the presence of an applied field of 0.5 T. The χ vs T and $\chi \cdot T$ vs T (where χ is molar magnetic susceptibility) plots are shown in Figure 7a. The $\chi \cdot T$ value decreases almost linearly from an initial value of 5.95 emu·mol^{-1}·K at 300 K to a value of ∼1.0 emu·mol^{-1}·K at 15 K, which suggests that the Mn centers are overall antiferromagnetically coupled in this complex. Below 15 K, $\chi \cdot T$ decreases sharply to a value of 0.23 emu·mol^{-1}·K at ∼2.0 K. Presumably, either intermolecular interactions and/or a sizable zero field splitting are responsible for this rapid decrease in the lower temperature range.

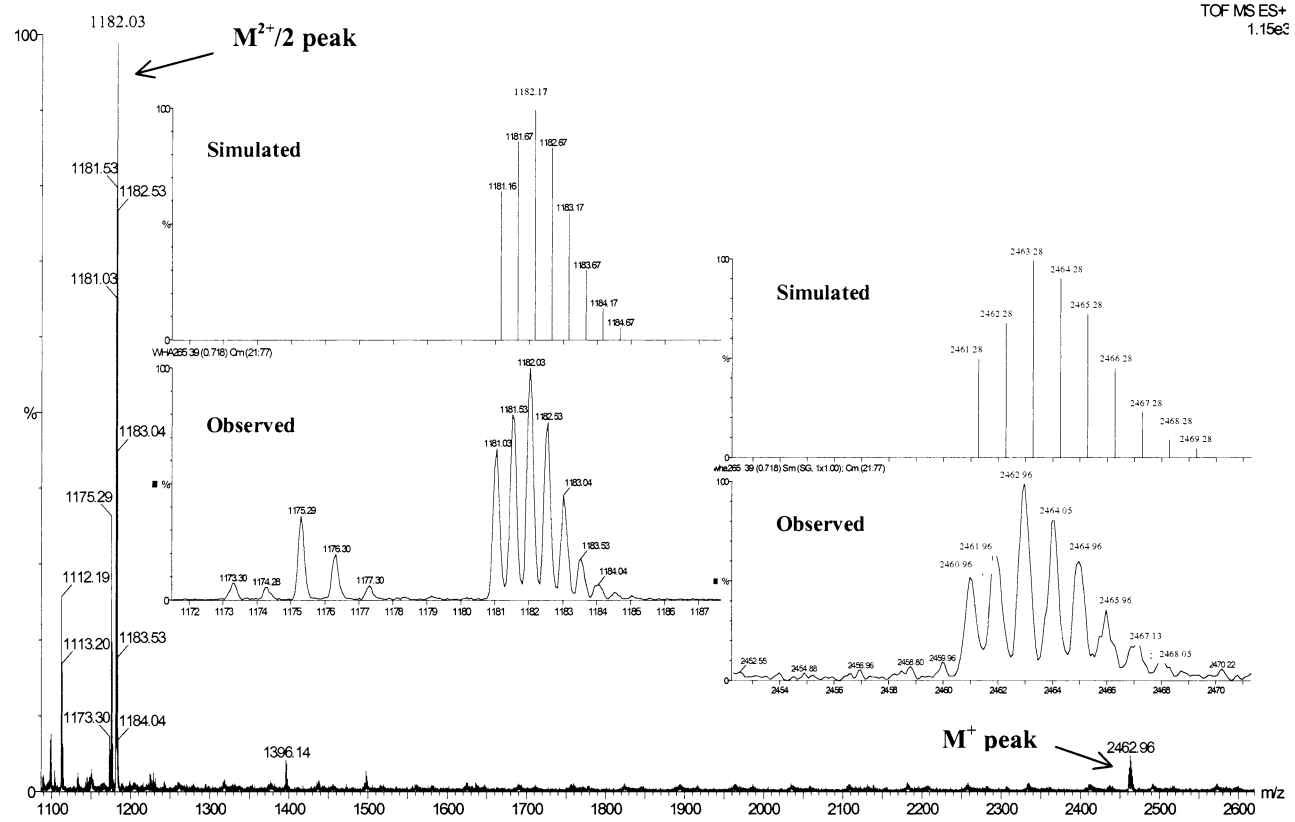

Figure 5. ESI MS Spectrum of **3**$(ClO_4)_4$.

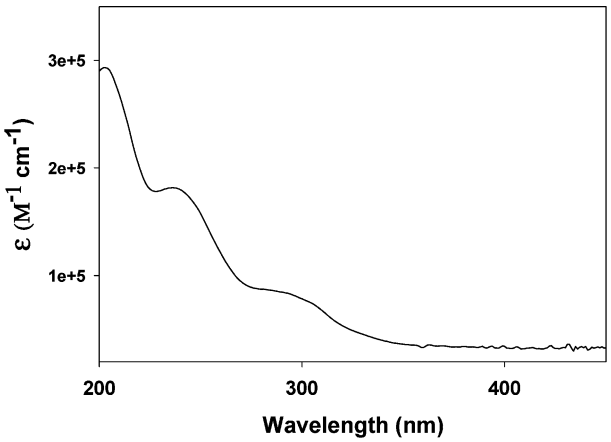

Figure 6. Electronic spectrum of **3** in acetonitrile.

It is evident from the structure that there are at least five significantly distinct Mn···Mn interactions present in the molecule. Application of the appropriate spin-Hamiltonian for this system yields a 6400 × 6400 spin-Hamiltonian matrix that is highly overparametrized. Clearly, a full solution of the magnetic properties of this complex system is nontrivial, requiring a complete matrix diagonalization procedure, which is beyond the scope of the present study.

Although it is not feasible to solve for individual pairwise magnetic interactions derived from the exchange Hamiltonian

$$H_{ex} = -2[J_{1,1A}(S_1 \cdot S_{1A}) + J_{1,2}(S_1 \cdot S_2) + J_{1,3}(S_1 \cdot S_3) + J_{1,3A}(S_1 \cdot S_{3A}) + J_{2,3}(S_2 \cdot S_3) + J_{3,1A}(S_3 \cdot S_{1A}) + J_{1A,2A}(S_{1A} \cdot S_{2A}) + J_{1A,3A}(S_{1A} \cdot S_{3A}) + J_{2A,3A}(S_{2A} \cdot S_{3A})]$$

quantitatively, it is useful to discuss them on the basis of literature precedents and relevant bonding considerations. One must keep in mind that a complete understanding of magnetostructural correlations for even simple dinuclear manganese complexes is lacking; therefore, some of the comments in the following paragraphs may be subject to alteration as work in this field continues to progress.

In the hexanuclear species described herein, two cuboidal Mn_3O_4 units are joined by Mn(1)−O(4A) and Mn(1A)−O(4) bonds. The trinuclear cuboidal half of the Mn_6 cluster, $Mn^{IV}_2Mn^{III}O_4$, is reminiscent of the cubane clusters $[Mn^{IV}Mn^{III}_3O_3X]^{6+}$ [44] and $[Mn^{IV}_2Mn^{III}_2O_4]^{6+}$ [45a] or $[Mn^{IV}_3Mn^{III}O_4]^{7+}$ [45b] with one manganese atom missing. In the distorted cubane-like Mn_4O_3X complexes, the $Mn^{III}\cdots Mn^{IV}$ exchange parameters, $J_{Mn(III)-Mn(IV)}$, have been reported to be antiferromagnetic in nature and range from −20.8 to −30.3 cm^{-1}.[44] Therefore, we hypothesize that the $Mn^{III}(3)\cdots Mn^{IV}(2)$ coupling in our complex is also antiferromagnetic and possesses a somewhat stronger exchange interaction ($100 > -J > 30$ cm^{-1}) owing to the presence of a μ-oxo bridge in addition to the aforementioned μ_3-oxo. The μ-oxo bridging ligand is known to promote strong exchange coupling in dimanganese(III,IV) complexes.[46a]

Additionally, the $Mn^{IV}(1)\cdots Mn^{IV}(2)$ interaction is also most likely antiferromagnetic and moderately strong with

(44) Hendrickson, D. N.; Christou, G.; Schimitt, E. A.; Libby, E.; Bashkin, J. S.; Wang, S.; Tsai, H.-L.; Vincent, J. B.; Boyd, P. D. W.; Huffman, J. C.; Folting, K.; Li, Q.; Streib, W. E. *J. Am. Chem. Soc.* **1992**, *114*, 2455−2471.

(45) (a) Ruettinger, W. F.; Campana, C.; Dismukes, G. C. *J. Am. Chem. Soc.* **1997**, *119*, 6670−6671. (b) Ruettinger, W. F.; Ho, D. M.; Dismukes, G. C. *Inorg. Chem.* **1999**, *38*, 1036−1037.

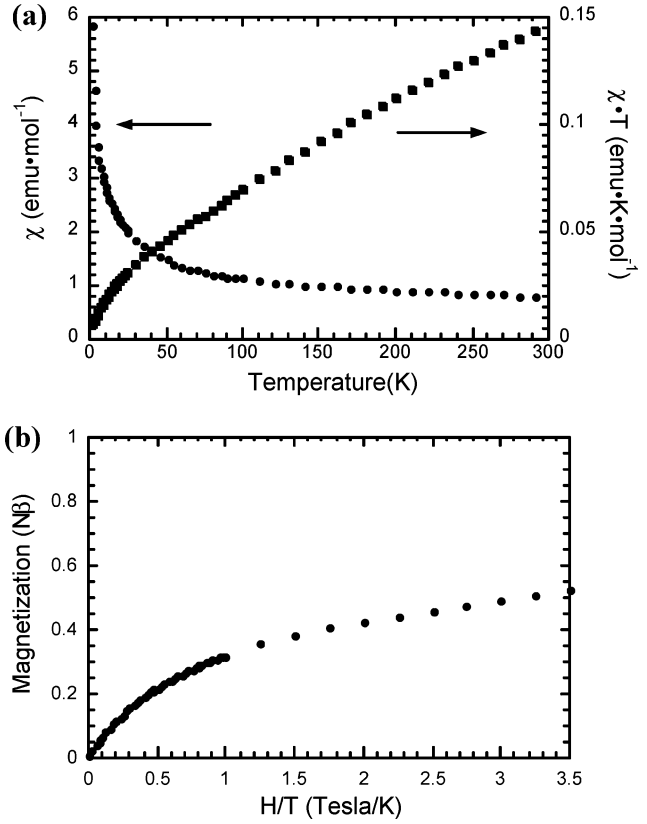

Figure 7. (a) χ vs temperature and $\chi \cdot T$ vs temperature and (b) isothermal magnetization vs magnetic field at 2.0 K for **3**$(OTf)_4$.

exchange interactions in the range $70 > -J > 30$ cm^{-1}. This is based on a magnetostructural correlation relating the Mn−O−Mn angle to the exchange parameter J, which has been developed recently for dinuclear complexes containing $\{Mn^{IV}_2(\mu\text{-O})_2\}$ cores.[46b] The $Mn^{IV}(1)-O(2)-Mn^{IV}(2)$ angle and Mn(1)−O(2), Mn(2)−O(2), and Mn···Mn distances in our complex are within the range found for these species, where the Mn(IV) centers are strongly antiferromagnetically coupled. In **3**, the magnitude of the $Mn^{IV}(1)\cdots Mn^{IV}(2)$ interaction is likely to be slightly weaker than that in isolated $\{Mn^{IV}_2O_2\}$ systems as the Mn(1)−O(1) bond is relatively long. However, we assert that a single short Mn−O−Mn bridging motif is sufficient to promote reasonably strong antiferromagnetic exchange coupling. This is supported by the J value obtained (−48 cm^{-1}) for $[Mn^{IV}_2(salpn)_2(\mu\text{-O})(\mu\text{-OH})](OTf)$ in which one of the core paths is long and the other short.[47] The interaction in the innermost dinuclear Mn(IV) moiety is taken to be fairly weak ($-J < \sim 30$ cm^{-1}) as they are bridged by two μ_3-oxo groups.

The $Mn^{III}(3)\cdots Mn^{IV}(1)$ coupling is likely to be antiferromagnetic and weak, owing to the long Mn(III)−(μ_3-O) bond involved in the exchange pathway. The dinuclear complex that most resembles this fragment is $[Mn^{III}Mn^{IV}(2\text{-OH-}3,5\text{-}Cl_2\text{-(SALPN)})_2(THF)](ClO_4)$.[48] Even though the $Mn^{III}(3)-O-Mn^{IV}(1)$ angles in our complex are much smaller (97° and 100.8° vs 126.7°), its J value of −10 cm^{-1} is a reasonable starting estimate for the corresponding subunit in **3**. The coupling between $Mn^{III}(3)$ and $Mn^{IV}(1A)$ is thought to be weak for the same reason, the long Mn(3)−(μ_3-O) axis length. A mono μ-oxo bridged dinuclear $Mn^{III,IV}$ species with an Mn−O−Mn angle of 125° was isolated by Wieghardt et al. and shown to have a J value of −40 cm^{-1}.[49] The exchange interaction between $Mn^{III}(3)$ and $Mn^{IV}(1A)$ in our complex is probably much weaker than that, and the sign is difficult to predict as these manganese centers are only coupled through a μ_3-oxo bridge with the Mn−O−Mn angle being quite large (158.6°).

Scheme 3. Schematic Diagrams of Mn_6 Core Showing (a) $S_T = 0$ and (b) $S_T = 4$ Ground State[a]

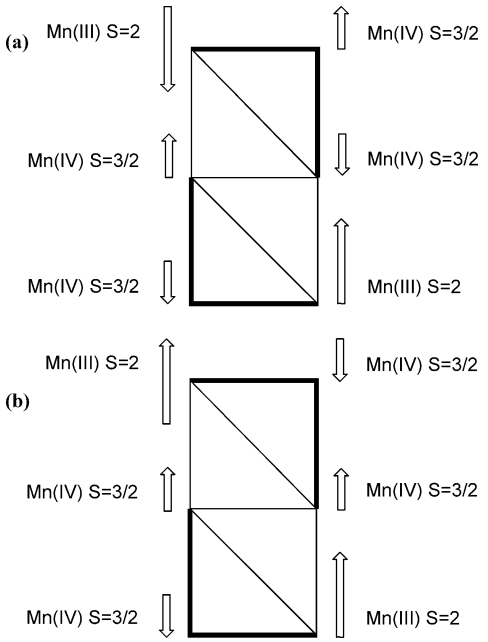

[a] The thick lines represent the strong antiferromagnetic exchange pathways based on the nature of the bridging ligands, bond distances, and angles, whereas the thin lines represent weaker exchange interactions.

On the basis of this discussion, two possible ground spin states, S_T, emerge for complex **3**, and these are illustrated using the diagrams in Scheme 3. In each cuboidal half, there are two dominant antiferromagnetic pathways, one between the two Mn(IV) centers and another between the terminal Mn(III) and Mn(IV) centers. These interactions would give rise to an $S' = 2$ spin state for each half of the cluster. Provided the two halves of the cluster antiferromagnetically couple with each other, this results in an overall $(S' + S') = S_T = 0$ spin ground state (as the case in Scheme 3a). On the other hand, provided the two cluster halves are ferromagnetically coupled, the ground spin state would become $S_T = 4$ (as in Scheme 3b).

A turnover in the χ vs T data, characteristic of cluster or chain compounds displaying $S_T = 0$ ground states, is not

(46) (a) Delfs, C. D.; Stranger, R. *Inorg. Chem.* **2001**, *40*, 3061−3076 and references therein. (b) Law, N. A.; Kampf, J. W.; Pecoraro, V. L. *Inorg. Chim. Acta* **2000**, *297*, 252−264.
(47) Baldwin, M. J.; Stemmler, T. L.; Riggs-Gelasco, P. J.; Kirk, M. L.; Penner-Hahn, J. P.; Pecoraro, V. L. *J. Am. Chem. Soc.* **1994**, *116*, 11349−11356.
(48) Larson, E.; Haddy, A.; Kirk, M. L.; Sands, R. H.; Hatfield, W. E.; Pecoraro, V. L.; *J. Am. Chem. Soc.* **1992**, *114*, 6263−6265.
(49) Wieghardt, K.; Bossek, U.; Bonvoisin, J.; Beauvillain, P.; Girerd, J.-J.; Nuber, B.; Weiss, J.; Heinze, J. *Angew. Chem., Int. Ed. Engl.* **1986**, *25*, 1030−1031.

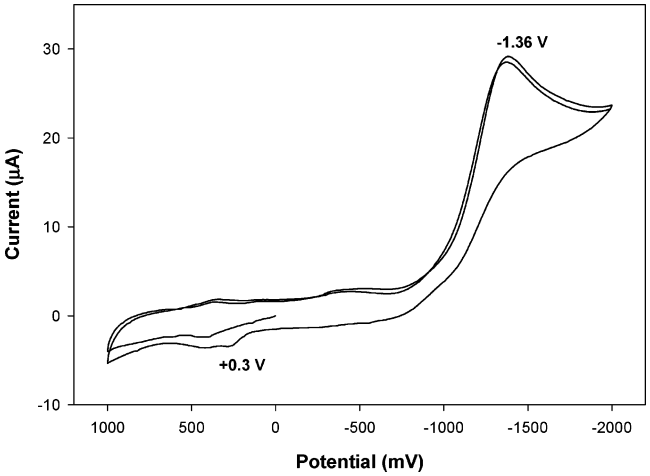

Figure 8. The cyclic voltammogram of **3**$(OTf)_4$ in acetonitrile showing both the anodic and cathodic scans of the complex.

observed for **3**. The most likely reason for the observed χ vs T behavior that is still consistent with a spin singlet ground state is the presence of $S_T > 0$ states, which are thermally populated at the lowest experimental temperatures (2 K). Inspection of the $\chi \cdot T$ vs T plot reveals that the $\chi \cdot T$ product tends toward zero as $T \rightarrow 0$. This is indicative of an $S_T = 0$ ground state and not an $S_T = 4$ ground state, where a value of $\sim$10 emu·mol^{-1}·K would be expected. Finally, isothermal magnetization data were collected between 0 and 7 T at a temperature of 2 K (Figure 7b). The magnetization values are quite low with a maximum of $\sim$0.5 $N\beta$ observed at 7 T. For example, a magnetization value of 1.0 $N\beta$ is anticipated for an $S_T = {}^1/_2$ system. Even at reasonably high applied magnetic fields, saturation was not achieved, which suggests that the complex possesses a low-energy $S_T > 0$ excited state(s) that is populated at $\sim$2 K. In summary, the susceptibility and magnetization data are most consistent with an $S_T = 0$ ground state assignment for the Mn_6 cluster.

Electrochemistry. A cyclic voltammogram of **3**$(OTf)_4$ in acetonitrile taken at a scan rate 100 mV/s, shown in Figure 8, displays an irreversible reduction at $E_P = -1.36$ V vs $Ag/AgClO_4$. The irreversibility could be attributed to a structural change of the complex or fragmentation upon reduction. A broad irreversible oxidation peak is observed at +0.30 V, which also appeared when the anodic scan was recorded before the cathodic scan. It is probably from a small impurity present in the sample as the current height is much lower compared to that of the reduction peak. The electrochemical behavior of complex **4** ($E_P = -1.45$ V) is similar to that observed for **3**. The redox behavior explains the chemical inertness of these complexes toward oxidation and reduction reactions with standard redox agents.

Complexes **3** and **4** are stable in the solid state and in solution under ambient conditions. Several Mn_6 clusters containing Mn(II) and Mn(III) centers were synthesized previously with acetate, pivalonate, and benzoate as carboxylate donor ligands.[24−27] These ligands have not yet been shown to stabilize higher oxidation states in hexanuclear manganese species. Recently, Christou and co-workers synthesized a hexanuclear manganese complex with the aid of a benzylic dicarboxylate ligand, *m*-phenylenedipropionate, with both Mn(III) and Mn(IV) ions.[50] Their complex is described as the superposition of two triangular units, one of them consisting of three Mn(III), whereas the other one has three Mn(IV) centers. Our complexes are the first to have four Mn(IV) and two Mn(III) atoms in a hexanuclear cluster and also are structurally very distinct from all other reported Mn_6 complexes. We speculate that not only the steric bulk, but also the electron donating effect, of these substituted benzoates helps to achieve such a novel core with the manganese centers in their high oxidation states.

Summary. This work demonstrates the application of sterically encumbering carboxylate ligands in synthesizing novel high-valent hexanuclear oxo-manganese clusters. These complexes have been characterized thoroughly by different physicochemical techniques including X-ray crystallography, ^{1}H NMR spectroscopy, electrochemistry, and dc magnetic susceptibility. Our ongoing efforts include attempts to link these Mn_6 units so as to form molecular solids, as well as to convert hexanuclear complexes to tetranuclear ones by the addition of Mn ions accompanied by Mn−O bond cleavage.

Acknowledgment. M.L.K. acknowledges the National Institutes of Health (GM-057378) and the Petroleum Research Fund (ACS PRF# 38086-AC3) for generous support of this research. We also thank Rosario M. Fico, Jr., at North Carolina State University for collecting the magnetic susceptibility data and Dr. Dongwhan Lee at Massachusetts Institute of Technology for providing useful suggestions regarding the ligand synthesis and purification. We are grateful to Chris Kowalczyk at Boston College for recording the mass spectral data. We thank Dr. Richard J. Staples at Harvard University for his valuable suggestions in modeling the disordered solvent molecules in the crystal structure.

Supporting Information Available: X-ray crystallographic data in CIF format for **1**$(OTf)\cdot 2CH_2Cl_2$, **2**$(OTf)\cdot CH_2Cl_2$, and **3**$(OTf)_4$. An ORTEP view of the cation of **2**. Table containing assigned ^{1}H resonances and chemical shifts for **3** and **4**. ESI mass spectra of **4**$(ClO_4)_4$, and μ_{eff} vs T plot for **3**$(OTf)_4$. This material is available free of charge via the Internet at http://pubs.acs.org.

IC034641H

(50) Cañada-Vilalta, C.; Huffman, J. C.; Streib, W. E.; Davidson, E. R.; Christou, G. *Polyhedron* **2001**, *20*, 1375−1380.